Bubble clustering and trapping in large vortices. Part 2: Time-dependent trapping conditions

Rade Ž. Milenković [a,*], Beat Sigg [b], George Yadigaroglu [b,c]

[a] *Laboratorium für Thermohydraulik, Paul Scherrer Institut, CH-5232 Villigen PSI, Switzerland*
[b] *Former Laboratorium für Kerntechnik, ETHZ, CH-8092 Zürich, Switzerland*
[c] *ETH WEN B-13, Weinbergstrasse 94, CH-8006 Zürich, Switzerland*

Abstract

In turbulent, periodically excited jets, interactions between bubbles and large coherent vortices are quantitatively studied. Simultaneous, two-phase PIV (particle image velocimetry) and photographic recordings were applied for tracking the large vortices and bubble structures and for investigating trapping phenomena. In order to quantify the interaction between bubbles and the large vortices that are formed in the shear layer, characteristic phase-averaged quantities were determined by PIV. The time-dependent vortex radius, the vorticity at the vortex centre and the time-dependent trapping conditions, obtained from the simulation of the vortex development, were tested against the experimental data.
© 2007 Elsevier Ltd. All rights reserved.

Keywords: Bubbly jets; Excited jets; Coherent structures; Bubble trapping; PIV; Optical probes; Phase averaging; Ensemble averaging

1. Introduction

In order to improve the understanding of complex gas–liquid systems and to bring forth new ideas for the development of advanced physical theories describing them, simple, basic experimental investigations with well-controlled conditions, designed for exploring transient and transitional and not only steady-state and fully-developed flow conditions, can be very useful. Such experiments can also play an important role in the formulation and development of models for turbulence and for phase interactions (closure laws), which represent key components of computational methods.

Bubbly jets are among the most effective ways for inducing gas-liquid mixing by injecting gas or vapor into liquid pools through nozzles, holes, tubes, etc. Such flows are characterized by the existence of large coherent vortical structures in the turbulent shear layers, which have significant effects on the spreading and dispersion of the bubbles. Furthermore, it is well-known that the way bubbles are dispersed plays a significant role and affects the overall efficiency of the processes involved.

---

* Corresponding author. Address: University of Applied Sciences – Northwestern Switzerland, Institute for Thermal and Fluid Engineering, Klosterzelgstrasse 2, CH-5210 Windisch, Switzerland. Tel.: +41 56 462 45 40; fax: +41 56 462 44 15.
E-mail address: rvmil@bluewin.ch (R.Ž. Milenković).

During recent years, a number of numerical (Sene et al., 1994; Yang et al., 2002, 2005; Wallner and Meiburg, 2002; Uchiyama, 2004) and experimental studies (Roig et al., 1998; Sun and Faeth, 1986a,b; Kumar et al., 1989; Stanley and Nikitopoulos, 1996; Iguchi et al., 1995, 1997) have been conducted that describe the dispersion of bubbles in plane as well as axisymmetric mixing layers. In these studies, the effects of bubble size and concentration on turbulence, the velocity and void distributions, shear layer spreading rates, mixing, the characteristic length scales and velocity correlations have been studied.

In bubbly flows, Uchiyama (2004) performed a three-dimensional simulation of a developing bubbly jet excited by periodical perturbations to study their effects on bubble dispersion. He found that the bubbles accumulate in the high-vorticity regions and that helical disturbances cause the largest dispersion of bubbles.

However, many experiments conducted with bubbly jets, bubbly plumes and bubbly mixing layers mainly provide results for statistical properties and the spatial distribution of local stochastic variables and do not investigate spatial coherence and the effects of large structures (vortices), which are very important in shear layers and have been extensively analyzed in single-phase flows (Crow and Champagne, 1971; Zaman and Hussain, 1980; Hussain and Zaman, 1980, 1981; Huerre and Monkewitz, 1985).

The authors of this paper have recently reported experimental work on interactions between bubbles and large vortices in round, excited bubbly jets (Milenkovic et al., 2005). Advanced techniques such as PIV (Particle Image Velocimetry), LIF (Laser-Induced Flourescence) and synchronized photographic recording were used. The basic idea of their experiment (Milenkovic, 2005) was to create large, orderly structures in a bubbly jet with controllable frequency and phase, in order to enable their study by statistical means and to provide clear conditions for investigating the interactions between the dispersed (bubbles) and the continuous phase (liquid) in two-phase jet flow. Periodical excitation of the jet at frequencies in the neighbourhood of those of its natural instabilities was applied to systematically create large coherent vortical structures and to demonstrate their importance. When bubbles enter such vortices, they can be trapped if certain conditions are fulfilled (see Part 1, Milenkovic et al., 2007).

In this Part 2 the variation of the trapping condition along the flow field and the escape of the bubbles from the large vortices further downstream are studied. The stronger dispersion of bubbles and the destruction of large coherent structures are characteristics of bubbly jets where buoyancy plays an important role. In the following sections, the time dependence of a Gaussian vortex is mathematically analyzed first, and the downstream dependence of the trapping condition is correspondingly formulated. This analytical dependence is then confronted to experimental results. The data presented here can be very useful for CFD-code validation, especially LES calculations.

2. Experiment

The experiments were carried out with a vertical water jet containing bubbles of various well-controlled sizes and volume fractions (Milenkovic and Fehlmann, 2005). The jet was injected into a large water pool to minimize wall effects. Jets that were periodically excited with controlled frequency and amplitude are called triggered jets here. The excitation was achieved by periodically modulating the jet shear layer by means of a coaxial water layer (EF) injected close to the jet exit through a separate annular nozzle (see Fig. 2 in Part 1, Milenkovic et al., 2007). More details about the experiments and the setup can be found in the first part of this paper (Milenkovic et al., 2007) and in Milenkovic (2005).

3. Time dependence of Burger's (Gaussian) vortex and trapping conditions

For the derivation of a trapping criterion (see Part 1 of this paper, Milenkovic et al., 2007), a simplified cylindrical vortex with its axis normal to the buoyancy direction was considered and the forces acting on a single bubble were formulated. Trapping of the bubble was then defined as the existence of an equilibrium position of the bubble inside the vortex.

Following the development in Part 1, it is assumed that the vorticity ω_z has an approximately Gaussian shape. Insertion of corresponding solution for U_φ (see Eq. (3) in Part 1 of this paper, Milenkovic et al., 2007) together with $U_r = U_z = 0$ into the time-dependent, viscous Navier–Stokes equation leads to the following results for the time-dependent vortex radius and the peak vorticity:

$$R_v^2(t) = R_v^2(t_0) + 4v \cdot (t - t_0) \tag{1}$$

$$\omega_0(t) = \omega_0(t_0) \cdot \frac{R_v^2(t_0)}{R_v^2(t_0) + 4v \cdot (t - t_0)} \tag{2}$$

Since the effective vortex radius $R_v(t)$ is a time-dependent function now, the functions $f_1\left(\frac{r}{R_v}\right)$ and $f_2\left(\frac{r}{R_v}\right)$ which appear in the equations for the equilibrium point of a bubble trapped in a vortex (see Part 1, Eqs. 19 and 20), are also time-dependent. Therefore, with Eq. (2), one obtains for the time-dependent parameters Γ_ω and Fr_ω

$$\Gamma_\omega(t) = \frac{\omega_0(t) \cdot R_v(t)}{V_T} = \frac{\omega_0(t_0) \cdot R_v(t_0)}{V_T} \cdot \frac{R_v(t_0)}{R_v(t)} = \Gamma_\omega(t_0) \cdot \frac{R_v(t_0)}{R_v(t)} \tag{3}$$

$$Fr_\omega(t) = \frac{\omega_0^2(t) \cdot R_v(t)}{4 \cdot g} = \frac{\omega_0^2(t_0) \cdot R_v(t_0)}{4 \cdot g} \cdot \frac{R_v^3(t_0)}{R_v^3(t)} = Fr_\omega(t_0) \cdot \frac{R_v^3(t_0)}{R_v^3(t)} \tag{4}$$

The time-dependent coordinates of the equilibrium position of a bubble trapped inside the vortex, $r(t)$ and $\varphi(t)$, can be obtained from the following equations:

$$\sin^2 \varphi(t) + \cos^2 \varphi(t) = Fr_\omega^2 \cdot f_1^2\left(\frac{r(t)}{R_v(t)}\right) + \Gamma_\omega^4 \cdot f_2^2\left(\frac{r(t)}{R_v(t)}\right) = 1 \tag{5}$$

and

$$\varphi(t) = \arcsin\left[\frac{\omega_0^2(t) \cdot R_v(t)}{4 \cdot g} \cdot f_1\left(\frac{r(t)}{R_v(t)}\right)\right] = \arcsin\left[Fr_\omega(t) \cdot f_1\left(\frac{r(t)}{R_v(t)}\right)\right] \tag{6}$$

or

$$\varphi(t) = \arccos\left[\frac{\omega_0^2(t) \cdot R_v^2(t)}{V_T^2} \cdot f_2\left(\frac{r(t)}{R_v(t)}\right)\right] = \arccos\left[\Gamma_\omega^2(t) \cdot f_2\left(\frac{r(t)}{R_v(t)}\right)\right] \tag{7}$$

Eq. (5) is used for calculating the radius $r(t)$ of the equilibrium position.

For trapping, the conditions $\Gamma_\omega(t) > \Gamma_{\omega,\min}(t)$ and $Fr_\omega(t) > Fr_{\omega,\min}(t)$ (see Part 1), must hold, where:

$$\Gamma_{\omega,\min}(t) = \left(\frac{1}{Fr_b^2 \cdot \beta^2(t) \cdot f_1^2\left(\frac{r}{R_v} = 1\right) + f_2^2\left(\frac{r}{R_v} = 1\right)}\right)^{1/4} \tag{8}$$

$$Fr_{\omega,\min}(t) = \frac{Fr_b \cdot \beta(t)}{\left[Fr_b^2 \cdot \beta^2(t) \cdot f_1^2\left(\frac{r}{R_v} = 1\right) + f_2^2\left(\frac{r}{R_v} = 1\right)\right]^{1/2}} \tag{9}$$

with the Bubble Froude number

$$Fr_b = \frac{V_T^2}{2 \cdot g \cdot d} = \text{const.} \tag{10}$$

and the length scale ratio

$$\beta(t) = \frac{d}{2 \cdot R_v(t)} = \frac{d}{2 \cdot \left[R_v^2(t_0) + 4 \cdot v \cdot (t - t_0)\right]^{1/2}} \tag{11}$$

If $\Gamma_\omega(t)$ and $Fr_\omega(t)$ decrease below the minimum values, bubbles can no longer be trapped.

For turbulent flow, the total viscosity should be used instead of the kinematic viscosity v

$$v_{\text{tot}} = v + v_t \tag{12}$$

where v_t is a space-independent turbulent viscosity. If this quantity is a time-dependent function, a slightly different solution for $R_v(t)$ is obtained. If v_t is assumed to be proportional to the velocity scale and the length scale that characterize the Gaussian vortex, it can be expressed as

$$v_t = 4 \cdot C \cdot \omega_0(t) \cdot R_v^2(t) \qquad (13)$$

where the constant C has to be determined experimentally. The turbulent viscosity v_t is then constant if $\omega_0(t) \cdot R_v^2(t)$ is constant, as shown by Eq. (2). The factor 4 has been used in Eq. (13) to make the expression consistent with that of a mixing layer where $v_t = C \cdot \Delta U \cdot L$ assuming that $\Delta U \approx 2 \cdot \omega_0 \cdot R_v$ and $L = 2R_v$ (Rodi, 1984).

By combining Eqs. (1), (12) and (13), the constant C can be expressed as:

$$C = \frac{\dfrac{R_v^2(t) - R_v^2(t_0)}{4(t - t_0)} - v}{4\omega_0(t) \cdot R_v^2(t)} \qquad (14)$$

Obviously, the approach presented here has to be validated against experimental data.

4. Discussion of PIV results for triggered jets with large bubbles

The PIV results (Part 1, Milenkovic et al., 2007) presented here were obtained for a turbulent bubbly jet with a mean superficial liquid velocity at the nozzle exit $V_{jet} = 0.32$ m/s, homogeneous void fraction of 3.4% and bubble diameter d of about 4 mm. These are the same conditions as for the experiments discussed in Part 1, Section 6 of this paper. The triggering frequency f, which corresponds to a Jet Strouhal number $St = \frac{D \cdot f}{V_{jet}} = 0.84$, is however, now 3 Hz. The time dependence of the velocity of the excitation flow at the exit of the triggering nozzle is shown in Fig. 1; the amplitude of the excitation signal is now somewhat weaker. A detailed description of liquid and bubble structures is presented in the following sections. The special method (Milenkovic et al., 2005) that has been developed for tracking these structures, the *vortex tracking method*, was discussed in Part 1 of this paper.

4.1. Tracking of the bubble ring

The generation of a bubble ring that travels with the same velocity as the vortex ring is a clear indication of bubble trapping inside the vortex ring, as already discussed in Part 1 of this paper.

The velocity of the bubble ring was measured using the vortex tracking method reported by Milenkovic et al. (2005). The excited bubbly jet was illuminated by the PIV laser light and by additional back light. If
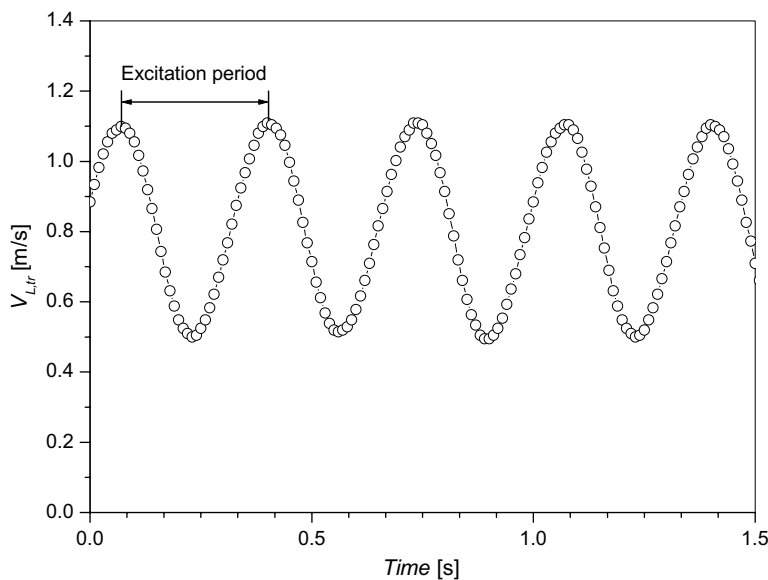
Fig. 1. Variation of the triggering velocity (3 Hz).
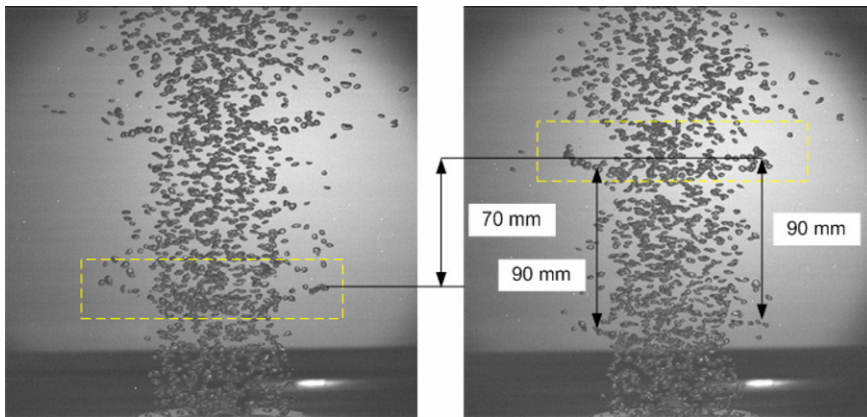
Fig. 2. Instantaneous images of the bubble ring (Left: starting phase P_1; Right: phase P_2, 267 ms later).

bubbles detected in the PIV images belong to a bubble ring, their phase-averaged velocity should be the same as the velocity of the vortex ring.

The photos of Fig. 2 representing two subsequent phases of the jet show the vertically shifted bubble ring. The vertical distance that the bubble ring travelled between phases P_1 and P_2 (see rectangles in Fig. 2), which are separated by a time shift of 267 ms, is about 70 mm. The instantaneous velocity of the bubble ring is about 0.26 m/s. On the other hand, the vertical distance of 90 mm between two bubble rings captured within the same phase (see picture on the right) corresponds to a velocity of 0.27 m/s, as the excitation period was 333 ms.

A phase-averaged photographic recording of bubble rings is presented in Fig. 3. This image was obtained by superimposing 30 frames obtained at the same phase and reveals the overall shape of the excited bubbly jet. Quantitative information cannot easily be obtained from this kind of data. Even though some clusters can be seen, trapped bubbles (i.e. bubble rings) are very difficult to distinguish. Further downstream, the bubble ring disintegrates when the trapping conditions are no longer fulfilled.
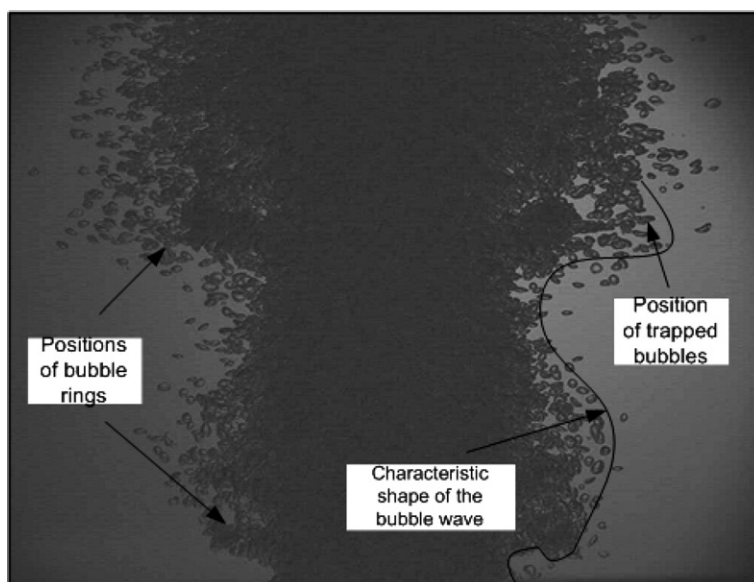
Fig. 3. Phase-averaged image of trapped bubbles (Phase P_1).

4.2. Downstream development of the vortex ring

This section contains experimental results obtained by the PIV vortex tracking method at two different camera fields of view that span elevations between $y/D = 0–2.4$ and $y/D = 2.4–4.4$, respectively.

Nine consecutive phases covering 1.6 excitation periods and showing the evolution of the jet and different locations of the vortex rings up to $y/D = 0–2.4$ from the nozzle exit are presented in Fig. 4. As the time between consecutive recordings was 66.7 ms and the excitation period was 333 ms, the sixth contour map of the phase-averaged vorticity of the liquid corresponds again to the beginning of the excitation period. The reproducibility of the data is well established by comparing these pairs of photographs at the same phase.

The data for the second phase presented in Fig. 4 (marked with number 2 – Phase 2), including phase-averaged velocities of the bubbles and of the liquid, as well as the azimuthal vorticity of the liquid, are analyzed and results are presented in Section 4.3. The vertical distance of 90 mm between two vortex rings
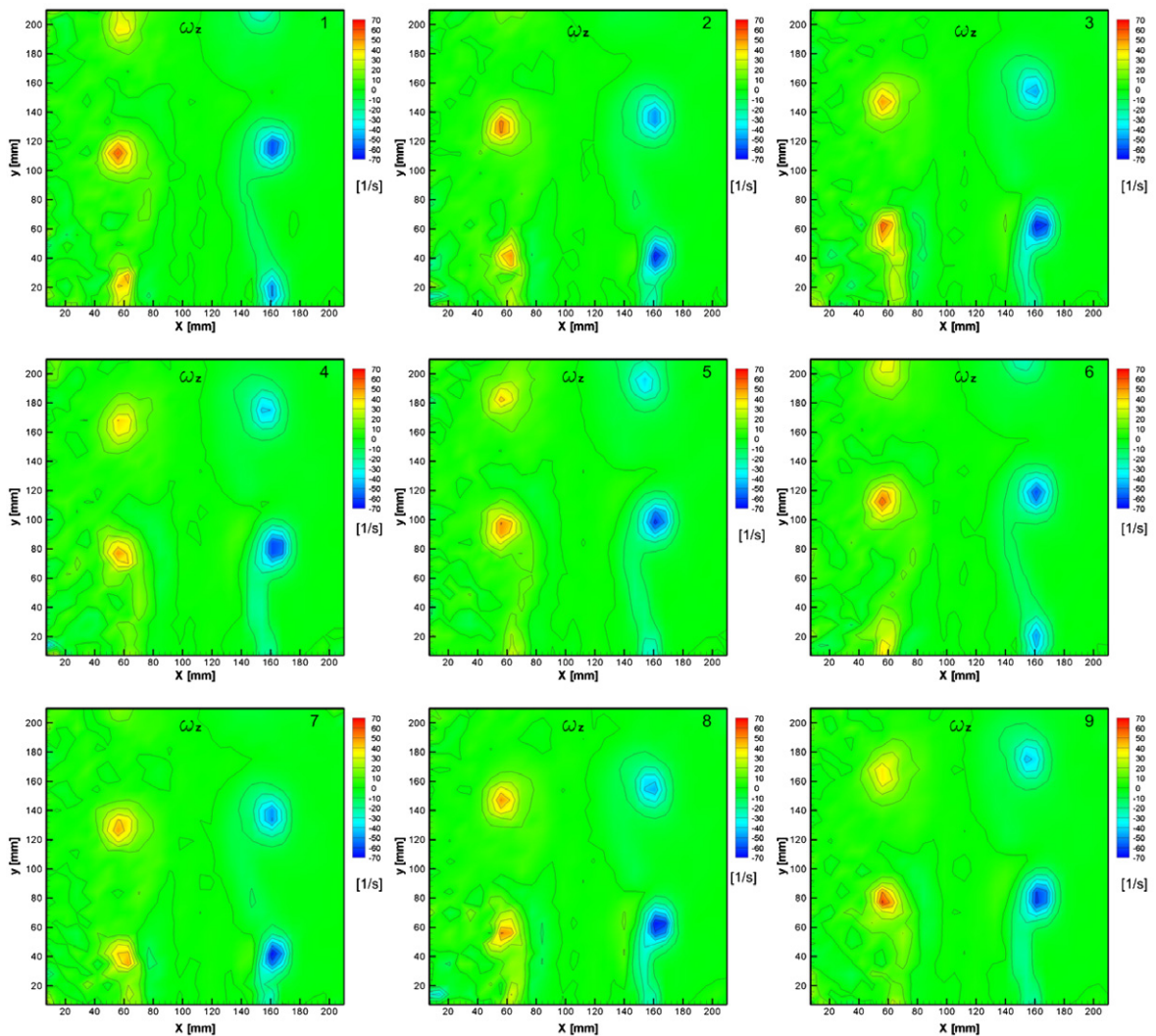
Fig. 4. Nine consecutive phases of the vortex ring movement obtained with the vortex tracking method near the nozzle, at $y/D = 0–2.4$. The time shift between the phases was 66.7 ms, or 1/5th of the triggering period. Consequently, phase 6 corresponds to phase 1, etc. The jet centerline is at $X = 108$ mm.

captured at the same phase (see Phase 2 in Fig. 4) corresponds to a velocity of 0.27 m/s, since the duration of the excitation period was 333 ms. Therefore, the PIV vortex tracking results provide consistent information on vortex ring and bubble ring velocities with that from the photographic bubble ring tracking.

The figures also show that the maximum vorticity in the vortex centre depends on the position of the vortex ring downstream from the nozzle exit. Close to the nozzle exit, the peak vorticity at the vortex centre is higher than further downstream, while the vortex diameter is smaller.

Data similar to those of Fig. 4 but obtained further downstream, between $y = 220$ and 400 mm ($y/D = 2.4$–4.4) are presented in Fig. 5. The sixth phase represents again the beginning of a new excitation period. The contour maps show the position and the size of the large vortices. The vortex centres of the first captured vortex ring are located at about 270 mm from the nozzle exit. The measured vortex ring velocity is about 0.37 m/s, which is considerably higher than the value obtained close to the jet nozzle.

The results illustrate the development and destruction of the vortex rings. The vorticity peak almost disappears at about $y = 405$ mm ($y/D = 4.5$) and vortex structures vanish at this location. This also affects the bubble distribution inside and in between the shear layer vortices. Gaussian velocity profiles and relative velocities of about the value of the terminal bubble-rise velocity characterize this region of the bubbly jet that is dominated by buoyancy; details can be found in Section 4.3 below and in the work of Milenkovic (2005).

4.3. Vortex properties time-dependent bubble trapping condition

This section contains the results on phase-averaged velocity and vorticity fields used to estimate the trapping parameters for a chosen phase and to examine the time-dependent values of these quantities.

Profiles of vertical bubble and liquid velocity distributions across the vortex rings, as well as of the azimuthal vorticity of the liquid for Phase 2 of Fig. 4, are presented in Fig. 6. The results at the two different elevations can be compared. The corresponding vorticity contour map (Fig. 4) shows the downstream locations of two vortex rings captured in the field of view. The velocity profiles of Fig. 6 are across these two vortex rings at the corresponding sets of elevations (left and right figures). Photographs of the flow, similar to Fig. 2, also showed the existence of two bubble rings. Preliminary tests presented by Milenkovic et al. (2005) showed that the vortex rings are formed at about 30 mm above the nozzle exit, which means that bubble trapping can take place at this location.

In order to examine the time-dependent trapping conditions, it is necessary to capture the phases, i.e. position, size and intensity of the vortex rings that contain trapped bubbles. Indeed, the sizes of the vortices, as well as of the bubbles, and the maximum vorticity at the vortex centre during a given phase determine whether trapping conditions are fulfilled or not. As can be seen in Fig. 4, the second (or the seventh) captured phase contain the vortex ring at about $y = 40$ mm from the nozzle exit. The vertical velocity profiles of the bubbles presented in Fig. 6, left, close to the nozzle exit show the existence of a velocity valley near the vortex centre, whereas those of the liquid exhibit a peak. The phase-averaged pictures of bubble reflections (examined but not presented here) at these locations reveal the existence of a zone where there are only a few bubble reflections. Since bubbles follow a path around the vortex until they are trapped, there is a zone within the vortex structure that is not reachable for most of the bubbles and no bubble velocity measurements are possible in this region. The valley in the bubble velocity distribution which lies at the side of the vortex close to the jet boundary is therefore an artefact.

Bubble rings are formed after trapping. The bubbles then continue to travel together with the vortex structures and have the same velocity as the vortex rings. Further downstream, the spreading of the bubbly jet and the secondary instability of the large vortex rings (Hussain and Zaman, 1981), which are also affected by interactions between liquid and bubbles, influence the distribution of the bubbles in the shear layer and their escaping from the coherent structures.

The downstream development of the vortex structures, the effects of instabilities in the shear layer on bubble agglomeration and movement and the break-up of the bubble ring will be examined in more detail in the next section. The velocity distribution of the bubbles and of the liquid, as well as the vorticity of the liquid across the vortex rings which were situated at about 180 and 390 mm (Phase 4 in Fig. 5) are presented in Fig. 7.
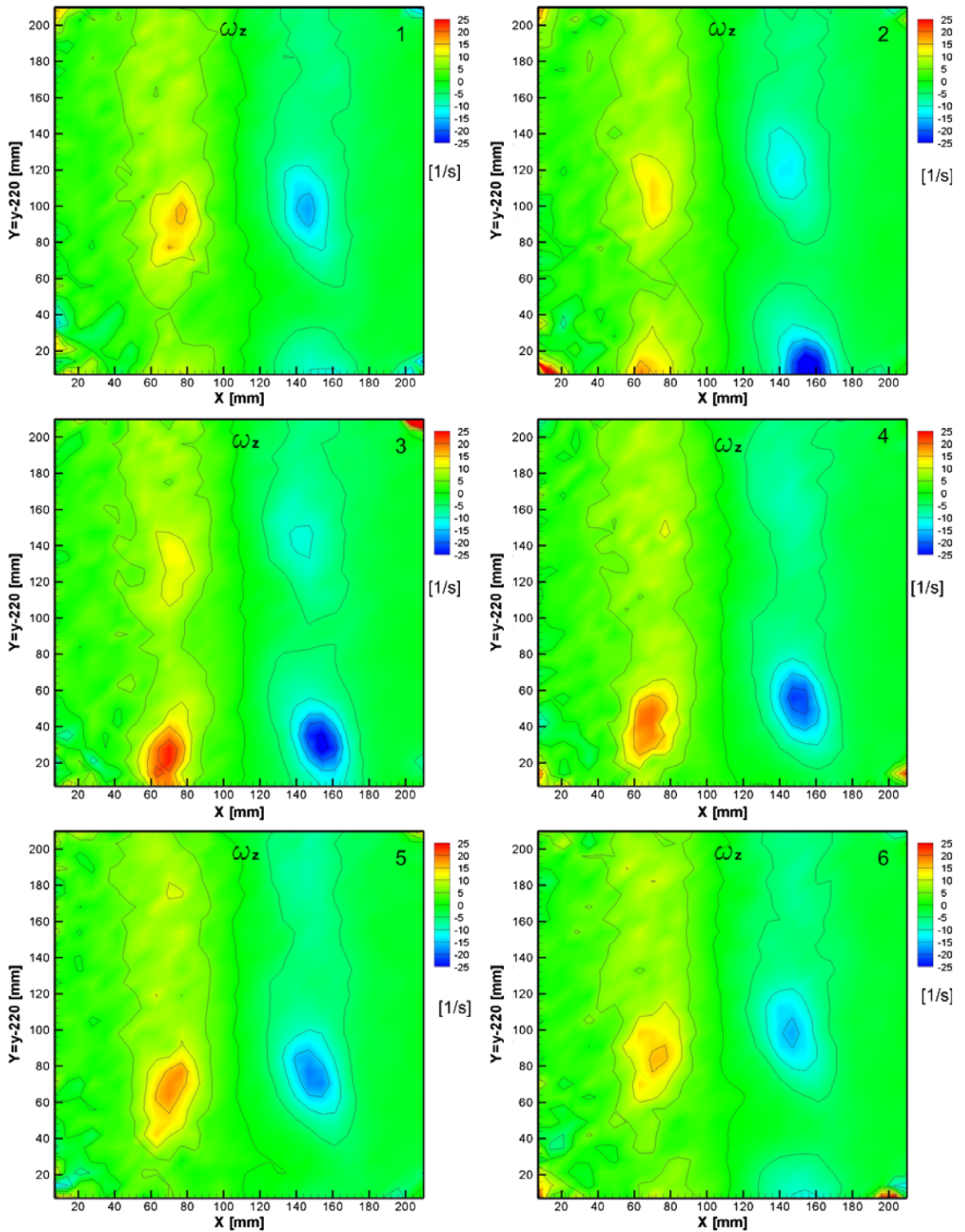
Fig. 5. Six consecutive phases of vortex ring movement obtained with the vortex tracking method at locations further downstream, $y/D = 2.4$–4.4. The time shift between the phases is 66.7 ms or 4/5th of the triggering period. The jet centreline is at $X = 108$ mm.
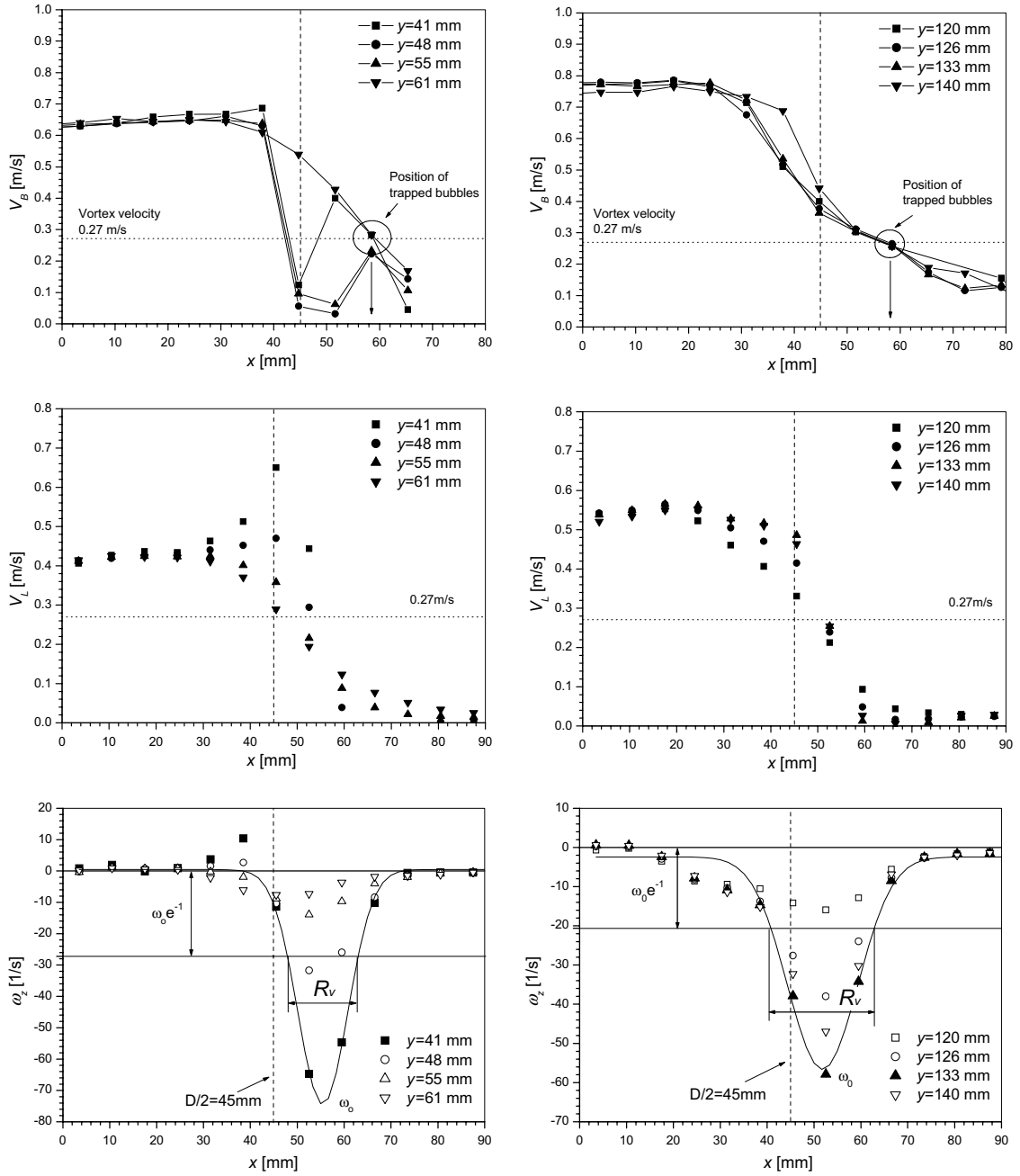
Fig. 6. Phase-averaged velocity profiles of the bubbles, and of the liquid, and azimuthal vorticity profiles of the liquid across the two vortex rings for Phase 2 of Fig. 5, at various elevations near the nozzle (left) and further downstream (right).

Horizontal profiles of the phase-averaged azimuthal vorticity through the centre of the vortex in the shear layer (shown in Figs. 6 and 7) are fitted by Gaussian curves:

$$\omega_z(x) = \omega_0 e^{-\frac{(x - x_c)^2}{R_v^2}} \tag{15}$$

where ω_0 is the vorticity at the vortex centre, R_v is the vortex radius and x_c is the horizontal location of the vortex centre. The vortex radius and vorticity at the vortex centre are experimentally-determined from the Gaussian fit as shown in Figs. 6 and 7.
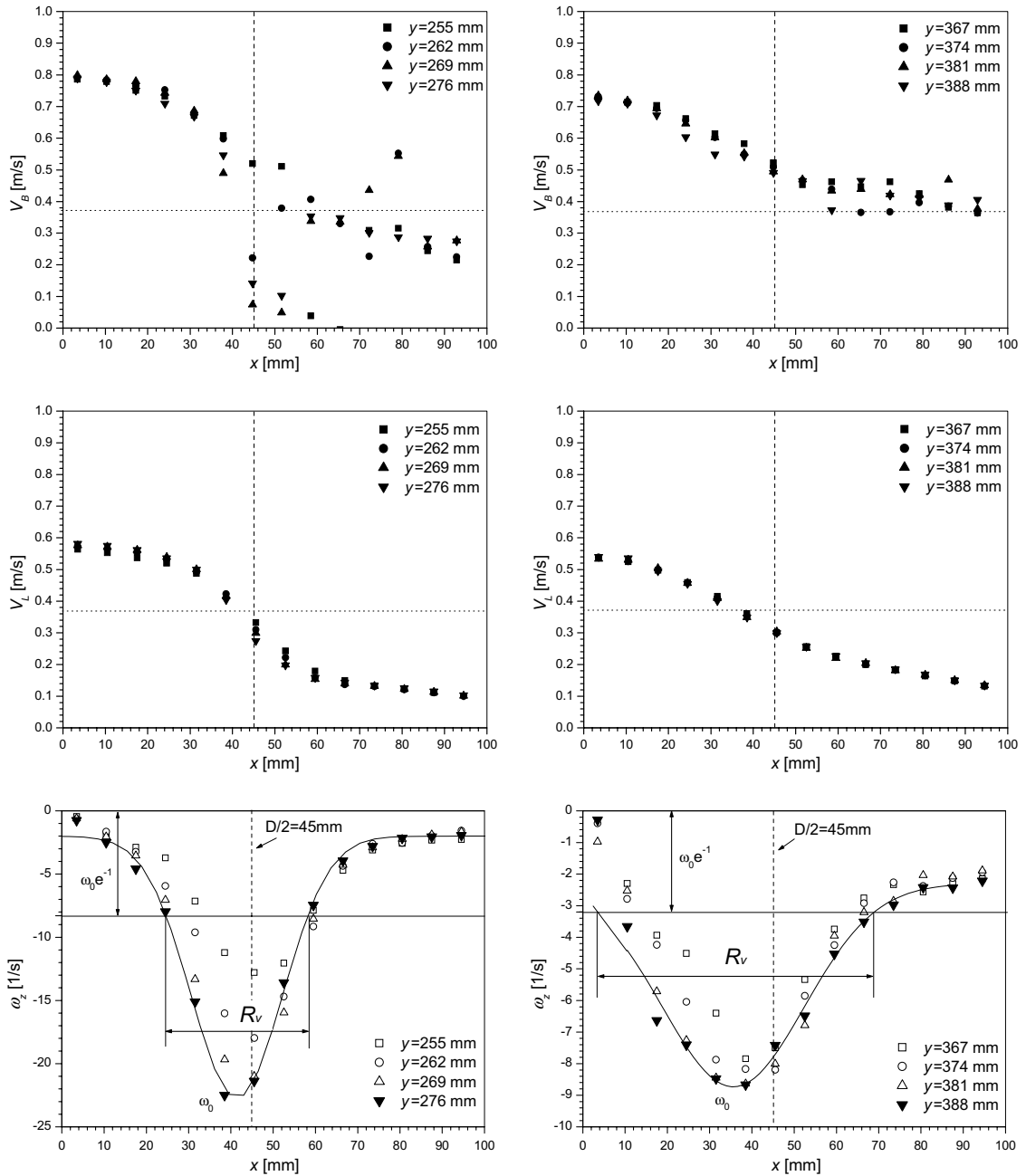
Fig. 7. Phase-averaged velocity profiles of the bubbles and of the liquid and azimuthal vorticity profiles of the liquid at elevations $y =$ 283–304 (left) and $y = 367$–388 mm (right) from the nozzle exit (phase 4 of Fig. 5).

The bubble and liquid velocity profiles also indicate that bubbles, driven by buoyancy, leave the vortex structures as the vortex travels downstream with a vertical velocity of 0.37 m/s and the phase-averaged vertical bubble velocity in the shear layer is about 0.46 m/s at $y = 381$ mm and $x = 50$–60 mm.

The experimental data for the vorticity at the vortex centre ω_0 and the vortex radius R_v as a function of the vertical elevation y (Fig. 8) show the development of the large coherent vortices in the shear layer.

The vorticity at the vortex centre decreases while the vortex radius increases. Obviously, bubble dispersion in the shear layer is also affected. The photo presented as Fig. 3 illustrates the characteristic shape of the
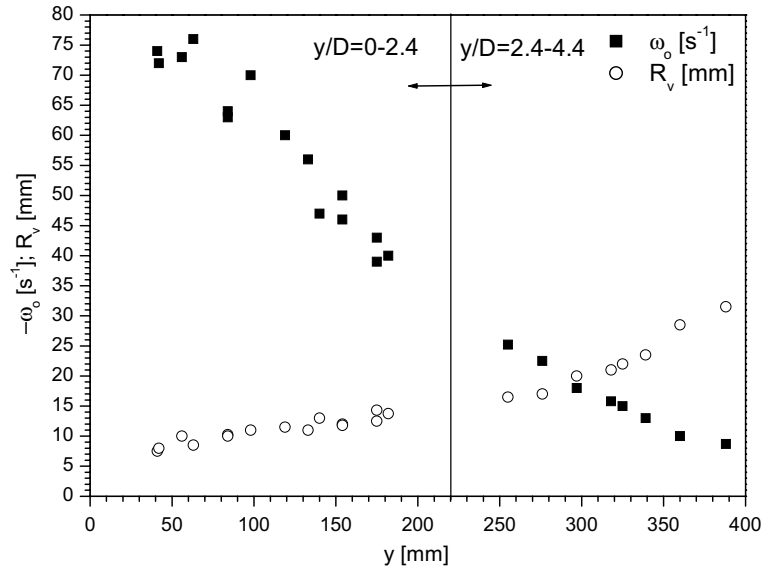
Fig. 8. Vorticity at the vortex centre and vortex radius experimentally determined at elevations $y/D = 0$–4.4.

bubble wave for the phase considered. As it can be seen, the dispersion of the bubbles increases further downstream.

The product $\omega_0 \cdot R_v^2(y)$ plotted in Fig. 9 shows that this quantity grows initially ($y \leqslant 50$ mm) and again for $y \geqslant 300$ mm; in between it is constant within the scatter of the data. During the growth phases, momentum is transferred from the jet to the vortices. The growth downstream of $y \geqslant 300$ mm may be a consequence of buoyancy, which accelerates the jet, and also the vortex velocity.

For the range 50 mm $\leqslant y \leqslant$ 300 mm, where $\omega_0 \cdot R_v^2(y) \approx$ const., Eq. (14) is applicable and a constant value for C results as $R_v^2(y)$ increases linearly with y, as it can be seen in Fig. 10. From a linear fit for $R_v^2(y)$ and the
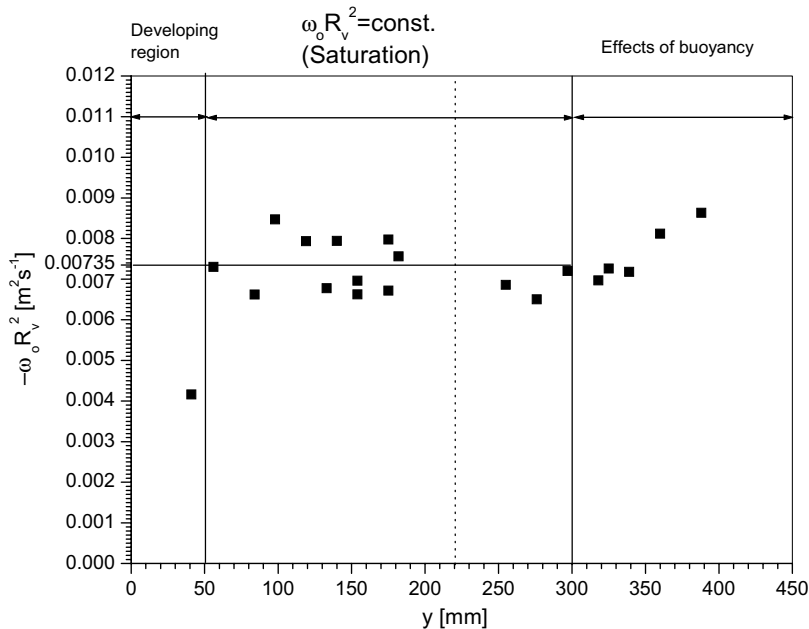
Fig. 9. Experimentally-determined quantity $\omega_0 \cdot R_v^2$ at different elevations y from the nozzle exit.
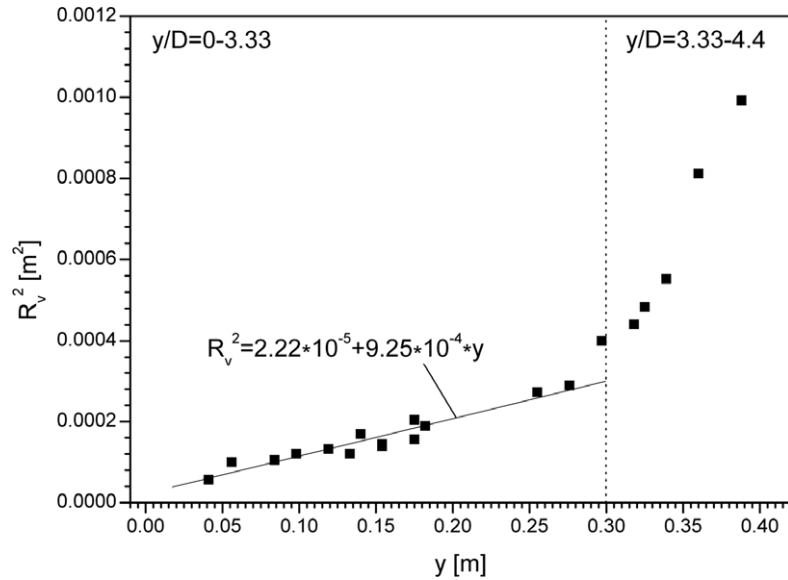
Fig. 10. Experimentally-determined quantity R_v^2 at different elevations y from the nozzle exit.

average value of $\omega_0 \cdot R_v^2(y)$ the value $C \approx 0.002$ results for this range. For $y > 300$ mm, the growth of $R_v^2(y)$ is much stronger according to Fig. 10.

Fig. 11 displays the vertical development of the non-dimensional quantities Γ_ω, Fr_ω, $\Gamma_{\omega,\min}$ and $Fr_{\omega,\min}$. The figure shows that downstream of $y/D \approx 1.33$, the trapping conditions are no longer satisfied. The photographic record presented in Fig. 2, however, illustrates that the bubble rings do not yet disintegrate completely at this elevation, but they are more deformed. Only further downstream, where the experimentally-determined trapping parameters are distinctly below the minimum values for trapping, the bubble rings start to disintegrate and bubbles are widely dispersed in the shear layer. It appears, therefore, that the bubble trapping conditions formulated in Part 1 (Milenkovic et al., 2007) are too stringent. One reason for this may be the too-high value
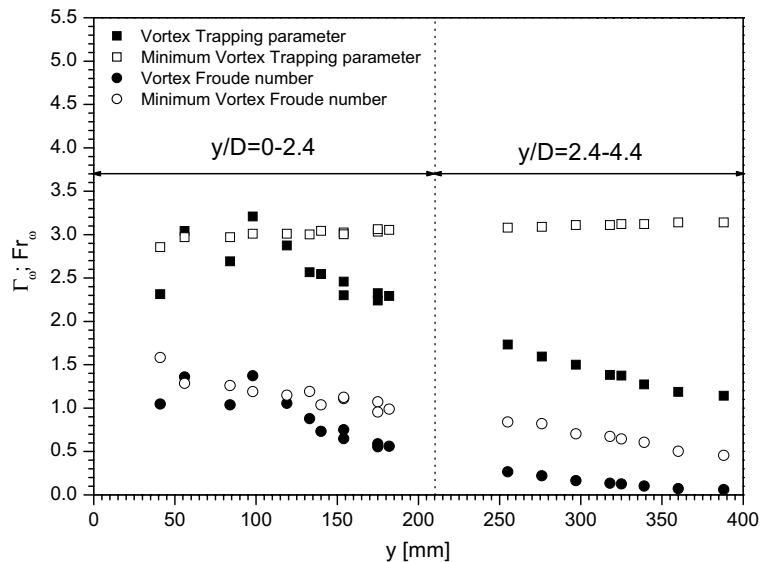
Fig. 11. Experimental results for the Vortex Trapping parameter and the Vortex Froude number obtained at elevations $y/D = 0$–4.4 ($C_l = 0.5$).
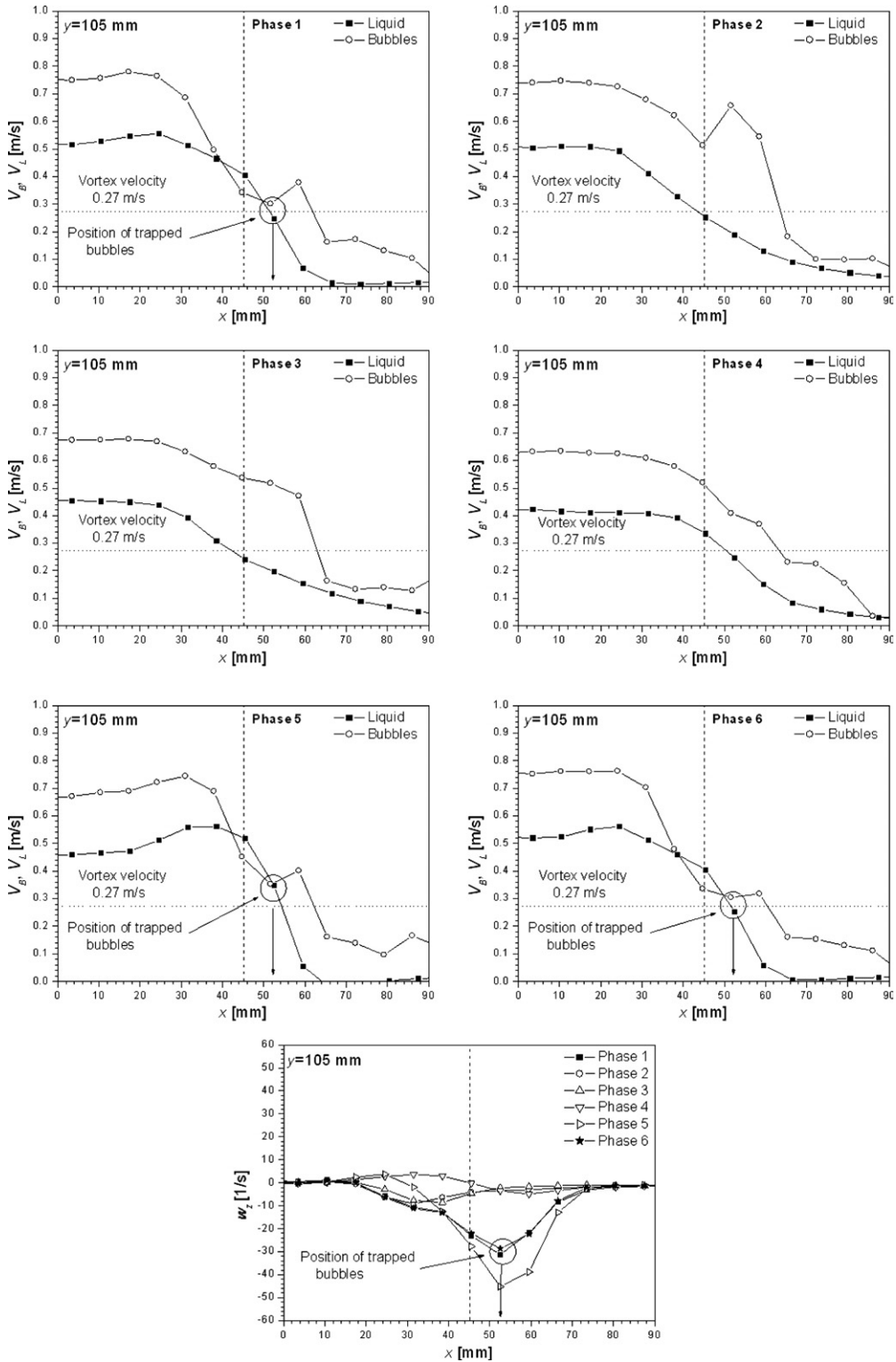
Fig. 12. Phase-averaged profiles of the vertical bubble and liquid velocity distributions and vorticity profiles of the liquid at $y = 105$ mm during six different phases.

of the lift coefficient ($C_l = 0.5$). As discussed in Part 1 and by Milenkovic (2005), it can be shown that a lower value for C_l leads to a decrease in $\Gamma_{\omega,\min}$ and $Fr_{\omega,\min}$.

5. Variation in time of the phase-averaged profiles

As already discussed in Part 1, if bubbles are trapped inside the vortex, they travel downstream at the same vertical velocity as the liquid in the vortex centre. In order to further verify this, phase-averaged bubble and liquid velocities are compared for six different phases (corresponding to the scalar maps of azimuthal vorticity distribution in Fig. 4). In addition, the liquid azimuthal vorticity obtained by PIV at $y = 105$ mm is also presented in Fig. 12.

In the first, as well as the sixth phase, which is the same as the first one, the centre of the vortex is located at about $x = 52$ mm ($X = 160$ mm) and $y = 115$–120 mm from the nozzle exit, as shown in Figs. 4 and 12. For these phases, results show that the vertical bubble velocity is larger than the vertical liquid velocity and the vortex velocity of 0.27 m/s, as expected. Taking into account that the vortex centre lies already above $y = 105$ mm for Phase 1 and that the equilibrium position of the trapped bubbles should be above the vortex centre (Milenkovic, 2005), it is not probable that trapped bubbles contribute to the bubble velocity results for Phase 1 presented in the profiles of Fig. 12.

On the other hand, the vortex centre in Phase 5 lies fairly close to $y = 105$ mm and trapped bubbles could be expected to mostly contribute to the velocity measurements in this phase. The corresponding values of the vertical bubble velocity and of the liquid velocity at the vortex centre in Phase 5 are, however, even higher than for Phase 1 (see Fig. 12).

Phase-averaged profiles of the vertical bubble velocity obtained by PIV may contain contributions from bubbles which move inside the large vortices but do not reach an equilibrium position. If the measured phase-averaged velocity of the bubbles is slightly higher than the vortex or liquid velocity, one may imagine that this is due to a small contribution of faster non-trapped bubbles or to measurement errors produced by the bubble size, which was relatively large compared to the interrogation areas of the PIV image fields. To elucidate such questions, high-speed visual recordings of bubble tracking and software for visual bubble tracking would have been needed, something that had to be left to future investigations.

6. Conclusions

Based on results presented in this paper, the following conclusions can be drawn:

- Because of the growth of the coherent vortices and due to secondary instabilities, the rings formed by trapped bubbles disintegrate at some distance downstream.
- The simplified mathematical model used for the development of a Gaussian vortex correctly reproduces the evolution of the vortex in the range $50 \leqslant y \leqslant 300$ mm. The new time-dependent trapping conditions corresponding to those defined already in Part 1 (Milenkovic et al., 2007) were evaluated by means of experimental data obtained by the vortex tracking method. It appears that the trapping conditions are somewhat too stringent, as bubbles remain trapped beyond the elevation where the trapping parameters fall below the minimum required values.

References

Crow, S.C., Champagne, F.H., 1971. Orderly structure in jet turbulence. J. Fluid Mech. 48, 547–591.
Huerre, P., Monkewitz, P.A., 1985. Absolute and convective instabilities in free shear layers. J. Fluid Mech. 159, 151–168.

Hussain, A.K.M.F., Zaman, K.B.M.Q., 1980. Vortex pairing in a circular jet under controlled excitation, Part 2, coherent structure dynamics. J. Fluid Mech. 110, 493–544.

Hussain, A.K.M.F., Zaman, K.B.M.Q., 1981. The preferred mode of the axisymmetric jet. J. Fluid Mech. 110, 39–71.

Iguchi, M., Okita, K., Nakatani, T., Kasai, N., 1997. Structure of turbulent round bubbling jet generated by premixed gas and liquid injection. Int. J. Multiphase Flow 23, 249–262.

Iguchi, M., Ueda, H., Uemura, T., 1995. Bubble and liquid flow characteristics in a vertical bubbling jet. Int. J. Multiphase Flow 21, 861–873.

Kumar, S., Nikitopoulos, G.M., Michaelides, E.E., 1989. Effect of bubbles on the turbulence near the exit of a liquid jet. Exp. Fluids 7, 487–494.

Milenkovic, R., 2005. Experimental Investigation of Bubbly Jets, Doctoral Thesis No. 16206. ETH Zürich.

Milenkovic, R., Fehlmann, M., 2005. Gas/Liquid Injector (Mass and/or heat transfer apparatus and method for mass and/or heat transfer enhancement), pending European Patent (PSI and ETHZ patent application No. 2003P19217EP (F-5125)).

Milenkovic, R., Sigg, B., Yadigaroglu, G., 2005. Study of periodically excited bubbly jets by PIV and double optical sensors. Int. J. Heat Fluid Flow 26, 922–930.

Milenkovic, R., Sigg, B., Yadigaroglu, G., 2007. Bubble clustering and trapping in large vortices. Part 1: Triggered bubbly jets investigated by phase-averaging. Int. J. Multiphase Flow, X, XXX–XXX.

Rodi, W., 1984. Turbulence models and their application in hydraulics – a state of the art review. International Association for Hydraulic Research.

Roig, V., Susanne, C., Masbernat, L., 1998. Experimental investigation of a turbulent bubbly mixing layer. Int. J. Multiphase Flow 24, 35–54.

Sene, K.J., Hunt, J.C.R., Thomas, N.D., 1994. The role of coherent structures in bubble transport by turbulent shear flows. J. Fluid Mech. 259, 219–240.

Stanley, K.N., Nikitopoulos, D.E., 1996. Bubble measurements in a gas-liquid jet. Chem. Eng. Comm. 143, 1–22.

Sun, T.Y., Faeth, G.M., 1986a. Structure of turbulent bubbly jets-I. Methods and centerline properties. Int. J. Multiphase Flow 12, 99–114.

Sun, T.Y., Faeth, G.M., 1986b. Structure of turbulent bubbly jets-II. Phase property profiles. Int. J. Multiphase Flow 12, 115–126.

Uchiyama, T., 2004. Three-dimensional vortex simulation of bubble dispersion in excited round jet. Chem. Eng. Sci. 59, 1403–1413.

Wallner, E., Meiburg, E., 2002. Vortex pairing in two-way coupled, particle laden mixing layers. Int. J. Multiphase Flow 28, 325–346.

Yang, X., Huang, X., Rielly, C., Zouaoui, Z., Guo, L., 2005. The modifications of a plane mixing layer by condensed bubbles. Chem. Eng. Sci. 60, 6876–6886.

Yang, X., Thomas, N.H., Guo, L.J., Hou, Y., 2002. Two-way coupled bubble laden mixing layer. Chem. Eng. Sci. 57, 555–564.

Zaman, K.B.M.Q., Hussain, A.K.M.F., 1980. Vortex pairing in a circular jet under controlled excitation, Part 1, general jet response. J. Fluid Mech. 101, 449–491.